Influence of laser beam size on measurement sensitivity of thermophysical property gradients in layered structures using thermal-wave techniques

Chinhua Wang,[1,2,a)] Andreas Mandelis,[3] Hong Qu,[1,2] and Zhuying Chen[1,2]
[1]*Institute of Modern Optical Technologies, Suzhou University, Suzhou, Jiangsu 215006, People's Republic of China*
[2]*Key Laboratory of Modern Optical Technologies of Jiangsu Province, Suzhou, Jiangsu 215006, People's Republic of China*
[3]*Center for Advanced Diffusion Wave Technologies, Department of Mechanical and Industrial Engineering, University of Toronto, Ontario M5S 3G8, Canada*

(Received 25 October 2007; accepted 16 December 2007; published online 28 February 2008)

The influence of the photothermal laser source beam size on the measurement sensitivity of layered systems using photothermal radiometry (PTR) is presented. Based on an appropriate theoretical model, widely different behaviors of the photothermal amplitude and phase in terms of combinations of thermophysical properties (i.e., thermal conductivity and thermal diffusivity) between a thin coating and the substrate are observed. The beam size effect on PTR measurement sensitivity is theoretically examined and experimentally demonstrated using a carbonitrided C1018 steel sample. The experimental results of using a variable size laser beam for the carbonitrided C1018 sample validate the theoretical prediction, in which an expanded beam exhibits a much larger magnitude change in both amplitude and phase as a function of frequency than measurements with a focused beam. The fitted thermal conductivity and thermal diffusivity based on the assumed industrially relevant range of effective hardness case depth gives the approximate range of the change in thermal conductivity and thermal diffusivity of C1018 steels after the carbonitriding process. © *2008 American Institute of Physics*. [DOI: 10.1063/1.2872462]

I. INTRODUCTION

Photothermal (PT) techniques include a variety of detection schemes for an optical-source-induced temperature rise in condensed matter and/or in adjacent fluid/gaseous media. They include photoacoustic spectroscopy,[1] PT radiometry (PTR),[2] photopyroelectric thermal-wave cavity detection,[3] and PT deflection.[4] These techniques have become important nondestructive testing (NDT) methodologies for thermophysical property measurements as well as for surface/subsurface defect detection.[5–7] Among other applications, PT techniques have been successful not only in homogeneous material diagnostics but also in the NDT of composite (thin-film) structures. To perform PT measurements, an optical source must be used to generate thermal waves after absorption of the radiation by the material. Garcia *et al.*[8] and Bendada *et al.*[9] investigated the thermophysical properties of coatings thermally sprayed on carbon steel substrates and discussed the influence of the thermal properties of the coating on the sensitivity of the standing thermal wave generated interferometrically through spatial confinement within the coating. These authors used PT sources with broad beam profiles. The most apparent advantage of using a broad beam is the relative simplicity of the mathematical treatment of the thermal-wave field using a one-dimensional (1D) heat conduction model. It turns out that another very significant advantage is the more effective confinement of the standing thermal wave within the surface layer compared to narrow PT excitation beams (the object of this paper). However, a larger beam size usually requires a much higher laser power in order to maintain acceptable signal-to-noise ratios of PT measurements, a fact which makes the technology costly and often impractical for weakly absorbing materials. The effect of the beam spot size on the behavior of the thermal-wave field using different beam sizes has been studied and corresponding three-dimensional (3D) theoretical models have been developed for both homogeneous[10] and layered materials.[11] Salazar *et al.*[5] further reported measurements of the effective thermal diffusivity of layered materials using either pointlike or planar laser source schemes. The 3D measurement schemes extend the capabilities of PT techniques toward achieving higher spatial resolution and understanding the behavior of the thermal-wave fields generated in layered solids as a function of dimensionality, in addition to the enhancement of signal quality. The corresponding 3D models quantitatively address the link between beam size and thermal-wave propagation directional degrees of freedom (axial and radial), especially in the low modulation frequency range where thermal diffusion length is larger than, or comparable to, the beam spot size. However, in all reported studies, the important issue of PT detection sensitivity to thermophysical parameters in layered solids or to thermophysical parameter gradients in continuously inhomogeneous structures as a function of beam size has not been studied to date. In practice, for a given layered structure, especially when the thermophysical contrast between adjacent layers is weak, one question must be answered before any PT measurement: what beam size can yield maximal or optimal measurement contrast/sensitivity to discontinuities or gradients in thermophysical parameters, such as those encoun-

[a)]Electronic mail: chinhua.wang@suda.edu.cn.

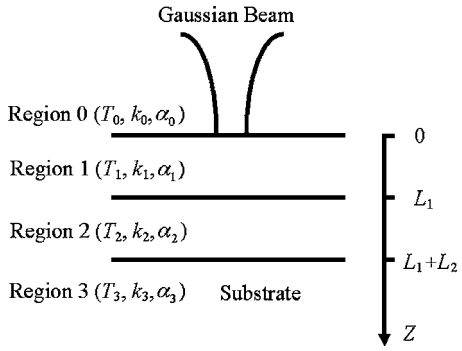

FIG. 1. Schematic cross section of a three-layer system for PT modeling.

tered in layered or surface engineered solids? This study has been motivated by the industrially driven need to evaluate nondestructively and/or reconstruct hardness case depth profiles in heat-treated steels using the PTR technique.[12,13] In this case of continuously varying mechanical and thermophysical depth profiles, the hardened steel sample can be treated as an effective double-layer (hardened layer +substrate) or a three-layer system (roughness layer +hardened layer+substrate) if the sample surface roughness is taken into consideration.[8,14] Due to the nature of heat-treatment-based hardening processes, the variation in thermophysical properties of the layers is very limited. To distinguish the small difference between layers and maximize PTR sensitivity of the hardened layer, selection of an appropriate laser beam size and spatial intensity profile is very important. Salazar *et al.*[15] discussed the beam size effect on the signal contrast of the PT mirage technique. They showed that the defocused pump beam leads to improved contrast in the case of layered structures and delaminations at the expense of compromised spatial resolution in the presence of cracks and small-size inclusions compared to the excitation beam size. In this paper, we will focus on the effect of source beam size optimization with respect to detection sensitivity of thermophysical gradients in layered structures where the upper layer is a thin film. It is shown that the sensitivity is not always enhanced with increasing beam size. In fact, for some medium beam sizes, depending on the relative physical properties of the two-layer system, the sensitivity could decrease as the beam size increases. We first develop a theoretical model that describes a three-layer structure and the corresponding thermal-wave field at the surface as detected using PTR. We then discuss the characteristics of such a system using various beam sizes and thermal properties of coating materials. Finally, we verify the model and prove its salient features using a case hardened (carbonitrided) C1018 steel sample. Quantitative changes in thermal properties of the hardened layer are determined based on PTR experimental data.

II. THEORETICAL MODEL

The geometry of the theoretical model is sketched in Fig. 1. The system consists of four regions with homogeneous and isotropic thermal properties [conductivity k_i, density ρ_i, specific heat c_i, and thermal diffusivity $\alpha_i(=k_i/\rho_i c_i)$, $i=0,1,2,3$]. The temperature in each region is denoted as $T_i(r,z,t)$ $(i=0,1,2,3)$. A semi-infinite substrate material (region 3) is assumed to lie underneath the two upper layers (regions 1 and 2 with thicknesses L_1 and L_2, respectively). The layered material is in thermal contact with the adjacent ambient (region 0). The lateral dimension of the sample (perpendicular to the z axis) is assumed to be extended infinitely or, in any case, much larger than the beam size and the thermal diffusion length in the frequency range of interest. The incident laser beam is assumed to be Gaussian with intensity distribution $[P/(\pi a^2)]\exp(-r^2/a^2)\exp(j\omega t)$ and is modulated at frequency $f=\omega/2\pi$, where P is the power of the incident Gaussian beam and a is the beam radius.

In this paper, we will focus on the study of a metallic coating system or any layered system that is opaque to the incident wavelength, in which the incident light is completely absorbed at the surface. With no bulk light absorption in the material, the thermal conduction equation in each region can be written as

$$\nabla^2 T_i(r,z,t) - \frac{1}{\alpha_i}\frac{\partial T_i(r,z,t)}{\partial t} = 0 \quad (i=0,1,2,3), \tag{1}$$

where the equation is expressed in cylindrical coordinates. The solutions of Eq. (1) are determined by boundary conditions at the three interfaces representing the continuity of temperatures and conservation of heat flux through the interface:

$$T_i(r,z,t) = T_{i+1}(r,z,t)\big|_z, \tag{2}$$

where $i=0,1,2$ for $z=0$, L_1, and L_1+L_2, respectively, and

$$k_i\frac{\partial T_i(r,z,t)}{\partial z} = k_{i+1}\frac{\partial T_{i+1}(r,z,t)}{\partial z}\bigg|_z, \tag{3}$$

where $i=1,2$ for $z=L_1$ and L_1+L_2, respectively. At $z=0$, conservation of thermal flux due to optical absorption can be expressed as

$$k_0\frac{\partial T_0(r,z,t)}{\partial z} - k_1\frac{\partial T_1(r,z,t)}{\partial z} = I(0,t), \tag{4}$$

where $I(0,t)$ is the surface thermal source and can be written as

$$I(0,t) = \frac{(1-R)PA_s\eta_s}{\pi a^2}e^{-r^2/a^2}e^{j\omega t}. \tag{5}$$

Here, R is the surface reflectivity, A_s is the surface absorptance, and η_s is the nonradiative energy conversion efficiency of the laser irradiated material.

Due to the cylindrical symmetry of the problem, the thermal-wave equations can be solved using Hankel transform techniques. After some algebraic manipulation, the solutions for the temperature rise in each region can be obtained. In particular, the surface temperature at $z=0$, which is detected in PTR, can be expressed as follows:

$$T_1(r,0) = Q_s(0)\int_0^\infty \frac{1}{k_0\delta_0(1+b_{10})}\frac{1+Q_{321}e^{-2\delta_1 L_1}}{1-\gamma_{10}Q_{321}e^{-2\delta_1 L_1}} \times e^{-\lambda^2 a^2/4}J_0(\lambda r)\lambda d\lambda, \tag{6}$$

where the harmonic modulation term $e^{j\omega t}$ of the temperature

field is omitted in Eq. (6). $Q_s(0)=\eta_s A_s(1-R)P/2\pi$ is a constant related to the laser power and the surface properties of the material. λ is the Hankel variable in the radial direction. $\delta_i^2=\lambda^2+\sigma_i^2$, $\sigma_i=(1+i)\sqrt{\omega/2\alpha_i}$ $(i=0,1,2,3)$;

$$b_{ij}=\frac{k_i\delta_i}{k_j\delta_j}, \quad \gamma_{ij}=\frac{b_{ij}-1}{b_{ij}+1}, \quad (i,j=0,1,2,3), \tag{7}$$

$$P_{32}=\frac{1+\gamma_{32}e^{-2\delta_2 L_2}}{1-\gamma_{32}e^{-2\delta_2 L_2}} \quad \text{and} \quad Q_{321}=\frac{1-P_{32}b_{21}}{1+P_{32}b_{21}}. \tag{8}$$

Note that Eq. (6) can be easily reduced to that describing a homogeneous sample by simply assuming $k_1=k_2=k_3$ and $\alpha_1=\alpha_2=\alpha_3$.[16] Even though in most cases a two-layer model will suffice for a thin film on top of a substrate, with the three-layer model, we add the flexibility of analyzing more realistic cases, such as a naturally occurring roughness layer on top of the substrate and the thin-film layer. For example, in the industrial case hardened steel case, one frequently encounters a surface roughness layer plus an effective hardened layer on the substrate, a three-layer system.[14] The uppermost layer may have very different physical properties which impact the experimental results and require a three-layer approach. The three-layer model can be easily reduced to a two-layer model by setting $k_1=k_2$, $\alpha_1=\alpha_2$, and L_1+L_2, the total thickness of the thin film. Equation (6) gives the thermal-wave field at any point on the sample surface along the radial direction.

III. NUMERICAL SIMULATIONS

As shown in Eq. (6), the thermal-wave (modulated temperature) field is a complicated function of experimental parameters (modulation frequency, beam size, etc.) and thermal parameters (k_i, α_i) of the layered structure. To gain more physical insight into the characteristics of the thermal-wave field, it is instructive to perform some numerical simulations to understand the dependence of the thermal-wave field which is a complex value and must be dissolved into the amplitude and phase in order to compare with experimental data.

To simplify the understanding of a layered system, we will mainly focus on a two-layer system which consists of only a thin-coating layer and a substrate. The substrate is assumed to be a C1018 steel sample (composition: 0.14%–0.2% C, 0.6%–0.9% Mn) with thermal conductivity $k=51.9$ W/m K and thermal diffusivity $\alpha=13.6\times10^{-6}$ m^2/s.[17] The thermophysical properties of the thin coating ($k_c=k_1=k_2$ and $\alpha_c=\alpha_1=\alpha_2$) are assumed to be different from those of the substrate in order to examine the behavior of the thermal-wave field. Figure 2 shows the beam size effect of the amplitude and phase of a thin-coating/C1018 system and a comparison with the amplitude and phase of a homogeneous C1018 steel sample under the same illumination using different beam sizes. The thickness of the coating is 100 μm. The thermal conductivity and thermal diffusivity of the thin coating are assumed to be 65 W/m K and 17.14×10^{-6} m^2/s, respectively, representing a 25.24% and a 26.31% increase from the corresponding parameters of the substrate. The amplitude is self-normalized to its lowest

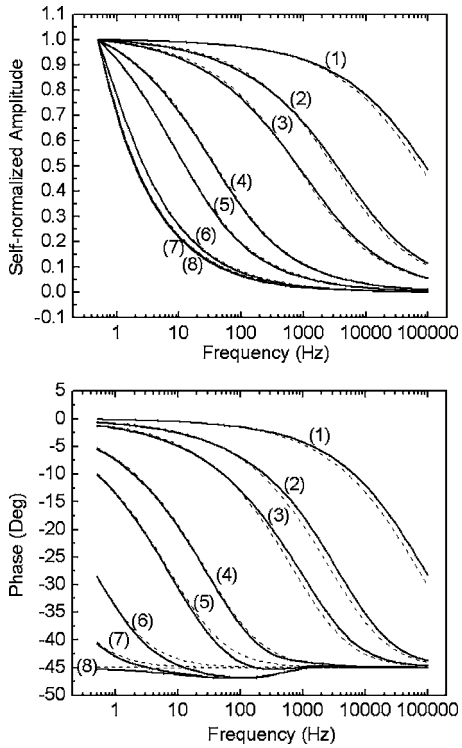

FIG. 2. Beam size effect on amplitude and phase of a homogeneous C1018 steel sample (dashed lines) and a thin-coating/C1018 system (solid lines) for several beam sizes. The thermal conductivity and thermal diffusivity of the thin coating are assumed to be 65 W/m K and 17.14×10^{-6} m^2/s, respectively. Beam size: (1) $a=0.01$ mm, (2) $a=0.05$ mm, (3) $a=0.1$ mm, (4) $a=0.5$ mm, (5) $a=1.0$ mm, (6) $a=4.0$ mm, (7) $a=10$ mm, and (8) $a=60$ mm. Coating thickness=100 μm.

frequency point at 0.5 Hz in each case. It is noted that the phase tends toward the −45° limit (independent of frequency) in the case of the homogeneous steel sample when the beam size is large (e^{-1} spot size $a=60$ mm), which is expected in the case of a 1D homogeneous sample (Ref. 16, Chap. 2.3, p. 90). It is seen that the differences between the homogeneous and layered systems, both in amplitude and phase, are buried within the dominating beam size effect. Any attempt to retrieve thermophysical information on the thin coating from such a beam dimensionality dominated signal will be compromised, which results in a very low detection sensitivity for monitoring thin coatings on substrates. The detection sensitivity at various beam sizes is hard to determine from the plots due to the small difference between the layered and homogeneous systems on the large y-axis scale of Fig. 2. To eliminate the dominating beam size effect on the detected signal and improve the resolution of the signal with respect to the thermophysical parameters of the coating, we introduce a normalization procedure in which the signal from a coating/substrate system is normalized (amplitude ratio and phase difference) by the substrate signal under identical measurement conditions. Figure 3 shows the amplitude and phase of the coating/substrate system normalized by the corresponding homogeneous steel sample described in Fig. 2. The large beam-dimension-related background signal is suppressed after normalization in both the amplitude and phase plots. The variations in both amplitude and phase channel are now purely due to the thermophysical contrast

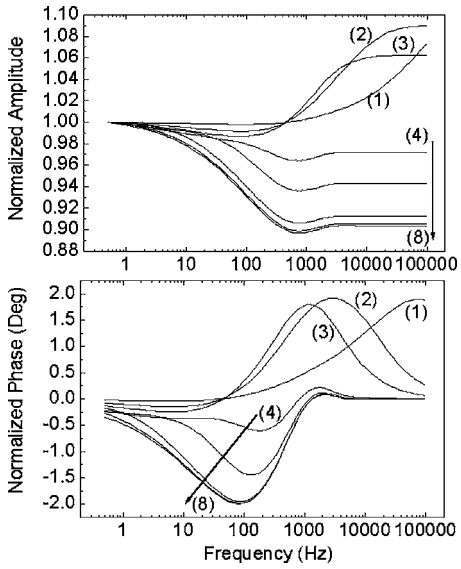

FIG. 3. Amplitude and phase of the coating/substrate system normalized by the corresponding homogeneous C1018 steel sample described in Fig. 2 using several beam sizes: (1) $a=0.01$ mm, (2) $a=0.05$ mm, (3) $a=0.1$ mm, (4) $a=0.5$ mm, (5) $a=1.0$ mm, (6) $a=4.0$ mm, (7) $a=10$ mm, and (8) $a=60$ mm. Coating thickness=100 μm; $k_c=65$ W/m K and $\alpha_c=17.14\times10^{-6}$ m^2/s.

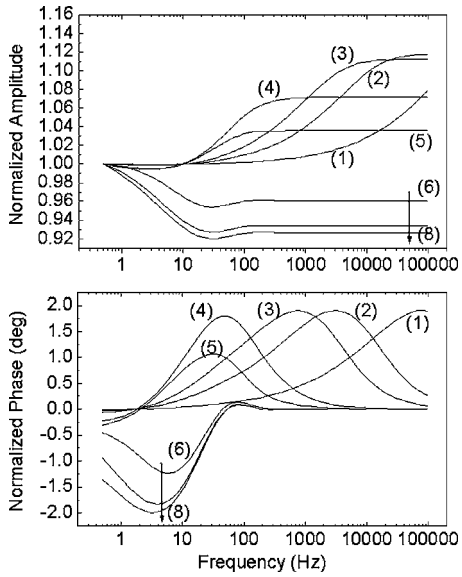

FIG. 4. Same as in Fig. 3 with coating thickness=500 μm; $k_c=65$ W/m K and $\alpha_c=17.14\times10^{-6}$ m^2/s.

between the layers. It is clear from Fig. 3 that the amplitude and phase show different behaviors as the beam size changes. When the beam size is small ($a<0.1$ mm), the feature peak in both amplitude and phase channel appears in a higher frequency range in contrast to the cases of a large beam size ($a>1.0$ mm) where the peak in the amplitude and phase moves toward the opposite direction in the lower frequency range. If we take a closer look at the evolution of the phase trough in the low frequency range as it is inverted to become the peak of the high frequency, we see that when the beam size increases, the magnitude of the trough shrinks until it disappears, while the peak at the high frequency end grows and eventually dominates for small beam sizes. The magnitude of the variation in both amplitude and phase also changes with beam size. In Fig. 3, both large (>4 mm) and small (<0.1 mm) beam sizes yield a large variation in amplitude and phase, while intermediate beam sizes (e.g., $a=1$ mm) yield a limited variation, which means low detection sensitivity in practice. It is also noted that the variation in the phase channel saturates when the beam size is less than 0.05 mm although the position of the peak changes. The same trend is seen when the beam size is larger than 10 mm: the valley saturates in the negative direction, as expected from 1D behavior. Figure 4 shows the overlayer thickness effect on the amplitude and phase under various beam sizes when the thickness of the film is increased (500 μm) compared to Fig. 3 (100 μm). While the basic features in Fig. 4 are similar to those in Fig. 3, the peak-to-valley positions, especially the valleys at low frequencies, shift toward lower frequencies. This can be easily explained by the larger thermal diffusion length at lower frequencies required to detect the thicker coating when compared to Fig. 3. Another interesting feature in Fig. 4, phase channel, is that the size of variation $\Delta\phi$ for a large beam size ($a=60$ mm, approximately 1D limit) is the same as that in Fig. 3 although the position of the peak is shifted due to the different coating thicknesses assumed in Figs. 3 and 4. It is seen that the magnitude of the phase minimum for large beam sizes corresponding to the 1D thermal-wave field is independent of the coating thickness and is solely determined by the thermophysical parameter differences between the coating and the substrate. This is consistent with the more conventional standing-wave patterns in propagating wave fields. The same phenomena are seen in the case of small beam sizes, for $a=0.01$ and 0.02 mm, where the phase in Fig. 4 saturates at the same level ($\sim1.90°$) as in Fig. 3. The saturated peak positions, e.g., the peaks in curves 1 and 2, however, remain unshifted with respect to the corresponding peaks in Fig. 3. This is different from the troughs in the lower frequency range discussed above, e.g., troughs in curves 6–8. The difference can be explained by the fact that at high frequencies, the thermal diffusion length is much shorter than the coating thickness (the upper layer is thermally thick); therefore, the PT signal arises solely from the coating material which can be considered as semi-infinite and thus the normalized phase tends to zero under 1D conditions, as expected.

In order to study the thermal-wave interferometric behavior of different types of coatings on the steel sample, we show three additional cases in which either the thermal conductivity, or the thermal diffusivity, or both of the coating are larger or smaller than those of the steel substrate. Figure 5 shows the case of $k_c=41.44$ W/m K and $\alpha_c=17.14$ m^2/s for the coating, representing the same percentage deviation from the parameters of the C1018 substrate but a decrease (−25.24%) in k and an increase (26.31%) in α. It is seen that when the beam size is small (e.g., <0.1 mm), both amplitude and phase in Figs. 4 and 5 show similar behavior, i.e., the normalized amplitudes of curves 1–3 show an increasing trend with frequency, while the phase peak is positive (phase lag). In fact, the magnitudes of the phase peaks of curves 1–3 in Figs. 4 and 5 are the same ($\sim1.90°$). The behavior of the

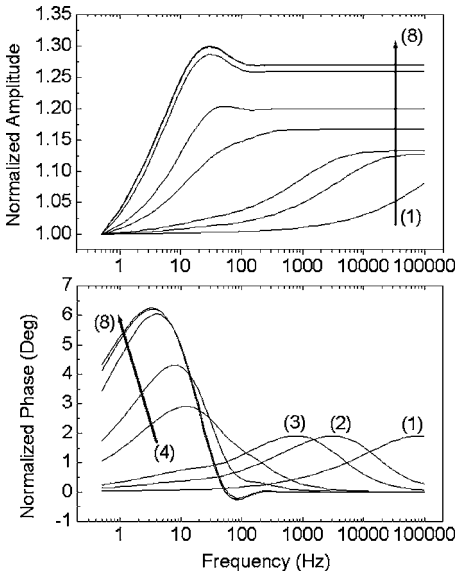

FIG. 5. Same as in Fig. 3 with coating thickness=500 μm; k_c=38.80 W/m K and α_c=17.14×10^{-6} m^2/s.

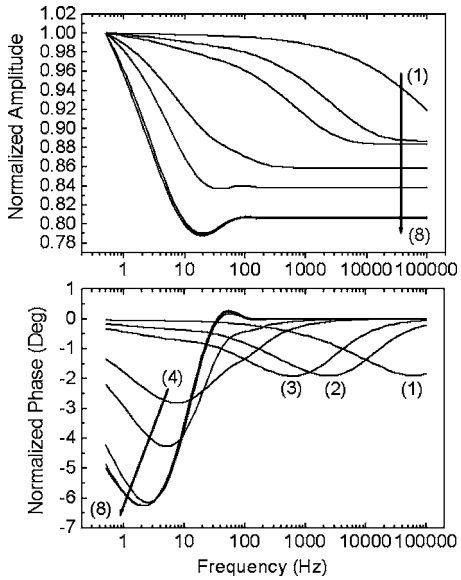

FIG. 6. Same as Fig. 3 with coating thickness=500 μm; k_c=65 W/m K and α_c=10.74×10^{-6} m/s^2.

amplitude and the phase under a large beam size (e.g., $a>1$ mm) is different. Here, both amplitude and phase exhibit opposite frequency trends. In Fig. 4, the normalized amplitude is less than 1 and also decreases with frequency until it saturates past the interferometric extremum, while the phase peak is negative (an interferometric "trough" or phase lead). In Fig. 5, the normalized amplitude is larger than 1 and increases with frequency until it saturates past the interferometric extremum, while the phase exhibits a positive peak. These effects are due to the relative differences in the thermophysical parameters (k and α) between the coating and the substrate, as they determine the standing thermal-wave pattern within the coating. In Fig. 4, the system parameters are k_c=65 W/m K, α_c=17.14×10^{-6} m^2/s for the coating and k_s=51.9 W/m K, α_s=13.6×10^{-6} m^2/s for the substrate, while in Fig. 5, the parameters are k_c=41.44 W/m K, α_c=17.14×10^{-6} m^2/s for the coating and k_s=51.9 W/m K, α_s=13.6×10^{-6} m^2/s for the substrate. The positive and negative Δk values between the coating and substrate create the results shown in Figs. 4 and 5, respectively. They affect the behavior of the amplitude and the phase using large beam sizes, but they do not affect the behavior of the amplitude and the phase using small beam sizes.

Similarly, Figs. 6 and 7 show two more combinations in which the parameters are k_c=65 W/m K, α_c=10.74×10^{-6} m^2/s for the coating and k_s=51.9 W/m K, α_s=13.610^{-6} m^2/s for the substrate (Fig. 6), and k_c=41.44 W/m K, α_c=10.74×10^{-6} m^2/s for the coating with k_s=51.9 W/m K, α_s=13.6×10^{-6} m^2/s for the substrate (Fig. 7). It is noted that the coating parameters assumed in all the systems (Figs. 4–7) represent approximately the same percentage deviations (±25.24% in k, ±26.3% in α), both increases (+) and decreases (−), from the C1018 steel substrate in k or α. This was done to observe changes in the frequency behavior of the PTR signal. Comparing Figs. 6 and 4, we note that in Fig. 6, the k_c of the coating is 65 W/m K (25.24% higher than the substrate), while α_c is lower (−26.3%). On the contrary, in Fig. 4, α_c is higher (26.3%) than α_s. The comparison shows that both amplitude and phase under a large beam spot size (>4 mm) exhibit the same behavior: the normalized amplitude shows a decrease with frequency away from unity and the normalized phase shows a trough of negative phase (phase lag). On the other hand, under a small beam spot size (<1 mm), the phase exhibits a positive peak (phase lead) in Fig. 4 and a trough (phase lag) in Fig. 6. The magnitudes of both deviations are approximately the same (~1.90°).

Next, a comparison of Figs. 5 and 7 is in order, where k_c is lower than k_s (−25.24%; opposite to Figs. 4 and 6), and α_c is, respectively, higher (Fig. 5) and lower (Fig. 7) than α_s by the same percentage. In a manner reminiscent of Figs. 4 and 6, both amplitudes and phases in Figs. 5 and 7 under a large

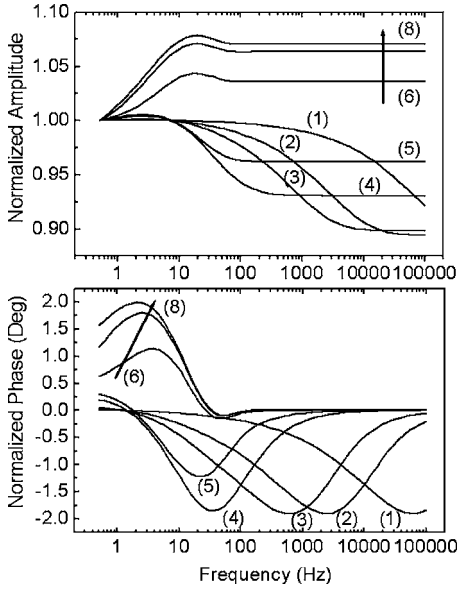

FIG. 7. Same as in Fig. 3 with coating thickness=500 μm; k_c=38.80 W/m K and α_c=10.74×10^{-6} m/s^2.

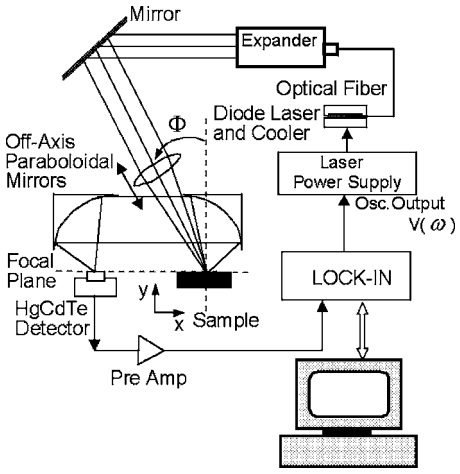

FIG. 8. Experimental setup for PTR of hardened steels.

beam size (>4 mm) follow the same trend owing to the same deviation in k_c, but they exhibit an increase in amplitude and a peak in phase with frequency, contrary to Figs. 4 and 6. The same behavior as in Figs. 4 and 6 can be seen in the frequency response under a small beam size: A positive phase peak (phase lead) is observed when the thermal diffusivity in the coating is higher than the substrate and a trough (phase lag) with the same magnitude as the peak appears when the thermal diffusivity of the coating is lower than the substrate. In all cases, Figs. 4–7, the effects of using smaller beam sizes appear in the higher frequency range, while those using larger beam sizes appear in the lower frequency range. In practice, however, the higher frequency range inherently suffers from the influence of surface conditions, such as roughness, contamination, porosity, and polishing processes which render the high frequency interference features practically useless as thin-layer diagnostic tools. From this point of view, the utilization of a larger beam size has the advantage over that of using smaller beam size. In view of Figs. 4–7, it should be noted that the use of an intermediate beam size (~2 mm) could lower the amount of change in the normalized amplitude and phase with changes in thin-layer thermophysical properties, thus compromising measurement sensitivity.

From Figs. 4–7, it is further seen that different amplitude and phase behaviors appear with different combinations of thermal conductivity and thermal diffusivity between the coating and the substrate. This can provide a fast approximate determination/evaluation of the relative physical parameters between the coating and the substrate based on the frequency behavior of the amplitude and the phase.

IV. EXPERIMENTAL AND RESULTS

To verify the foregoing theoretical considerations, PTR experiments were performed using a sample of carbonitrided C1018 steel (0.14%–0.2% C and 0.6%–0.9% Mn) with a flat surface. The sample was subjected to a standard industrial carbonitride hardening process, which resulted in a hardened case with depth ranging from a few micrometers to 1000 μm, depending on the conditions of the hardening process. The experimental system is shown in Fig. 8. The

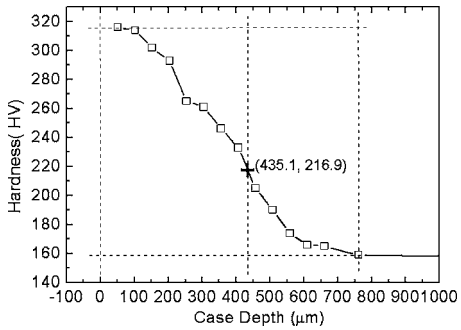

FIG. 9. Case depth profile of a carbonitrided C1018 steel sample measured with the mechanical indenter method.

thermal-wave source was a high-power semiconductor laser (~20 W). The output of the laser was modulated by a periodic current driver, the frequency of which was controlled by the computer and also served as the lock-in reference. The beam was expanded, collimated, and then focused onto the surface of the sample with a variable spot size ranging from ~1 to 20 mm by adjusting the position of the lens. The harmonically modulated infrared radiation from the sample surface was collected by an off-axis paraboloidal mirror system and detected by a wide bandwidth HgCdTe detector. The signal from the detector was amplified by a low-noise preamplifier and then fed into a lock-in amplifier which was interfaced to the PC.

The sample under test had undergone a nominal 0.02 in. case depth hardening. The case depth profile was determined by a conventional mechanical indentation method and is shown in Fig. 9. The hardness of the steel changed from 316 HV (Hardness Vickers) at the surface to ~160 HV at a depth of ~700 μm. The case depth at $1/e$ of the full depth is approximately 435 μm. The PTR frequency responses of the sample were then measured using a focused beam and an expanded beam, respectively. Figure 10 shows the measurement result of using a focused beam of radius a =0.725 mm. Figure 11 shows similar results using an expanded beam of radius a~20 mm. The beam sizes were measured with a pinhole (diameter ~5 μm) along two arbi-

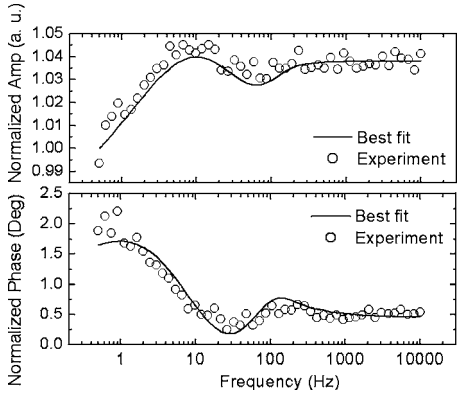

FIG. 10. Experimental amplitude and phase and theoretical best fits under a focused laser beam (a=0.725 mm). The thermophysical parameters of the AISI1018 steel substrate are assumed: k_s=51.9 W/m K, α_s=13.6 $\times 10^{-6}$ m^2/s. The thermal conductivity k_c and thermal diffusivity α_c of the effective hardened layer are fitted: k_c=29.4 W/m K and α_c=9.0$\times 10^{-6}$ m^2/s.

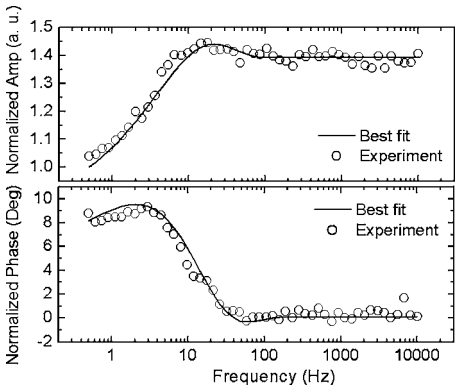

FIG. 11. Experimental amplitude and phase and theoretical best fits under an expanded laser beam (a=60 mm). The thermo-physical parameters of the AISI1018 steel substrate are assumed: k_s=51.9 W/m K, α_s=13.6 $\times 10^{-6}$ m^2/s. The thermal conductivity k_c and thermal diffusivity α_c of the effective hardened layer are fitted: k_c=26.0 W/m K and α_c=9.3$\times 10^{-6}$ m^2/s.

trary orthogonal directions (X and Y), followed by fitting to Gaussian profiles. For example, in the focused case, the fitted beam radii along the X and Y directions were 735.82 and 714.59 μm, respectively, resulting in an average beam size of a=725.21 μm. In both Figs. 10 and 11, the amplitudes and the phases were normalized with that of an unhardened C1018 flat steel sample with exactly the same beam size in order to eliminate the instrumental transfer function. It is seen that the thus normalized amplitude ratio and phase difference using the focused beam are much smaller than those obtained using the expanded beam. The normalized amplitude changes from 1 to ~1.05 in the case of a focused beam, whereas a much larger change, from 1 to ~1.5, occurs in the case of an expanded beam. The normalized phases show the same trend in which the peak-to-trough change is less than 2° with the focused beam but about 10° with the expanded beam. In conclusion, measurement sensitivity in both amplitude and phase is considerably more limited using a focused beam than an expanded beam.

The fact that very reasonable fits to the theoretical expression, Eq. (6), were obtained for the experimental results shown in Figs. 10 and 11 is remarkable because the case depth is not an abrupt surface layer, but its properties gradually and continuously change as a function of depth. Therefore, it can be concluded that one may use the two-layer PT theory to approximate the thermal-wave behavior of continuously varying depth profiles of steel hardness. This requires assuming an effective case depth and deriving the thermophysical properties (k_c, α_c) from the best fits. Having determined the effective thermophysical parameters of the case, comparing Figs. 10 and 11 with Fig. 7 leads one to easily deduced that both thermal conductivity and thermal diffusivity of the hardened layer are lower than those of the substrate (i.e., the unhardened C1018). This observation is consistent with results published before for the hardened steel samples.[12,13] However, in the earlier studies, the detailed hardness profiles of the hardened layers were taken into consideration within the framework of a more complicated (and realistic) inverse thermal-wave problem. The present results are very useful in the sense that continuously varying hardness depth profiles in C1018 steel behave as an *effective abrupt* thermal-wave boundary and the effective thermal thickness may be used as a criterion for estimating the case depth. In the fitting process, the known parameters of C1018 steel were used for the substrate [i.e., k_s=51.9 W/m K, α_s=13.6$\times 10^{-6}$ m^2/s (Ref. 17)], and the thermal conductivity and diffusivity of the hardened layer were set as adjustable parameters. In the case of a focused beam, the radial position of the measurement, i.e., the distance of the measurement point from the center of the incident Gaussian beam profile at the focal point, was also set as a fitting parameter. This is necessary because the PTR signal in three dimensions is a function of the radial position, r, of the oscillating temperature field as shown in Eq. (6). In the experiment, if the focal point of the paraboloidal mirror corresponds to both beam center and measurement spot, then one may set r=0; otherwise, r must be determined. In order to obtain the thermal parameters of the hardened layer, one also needs to know the *effective* case depth, which was assumed to be 435.1 μm based on the $1/e$ location in Fig. 9. The best-fitted thermal conductivity and diffusivity of the hardened layer using the focused beam and the expanded beam were 29.4 W/m K, 9.0$\times 10^{-6}$ m^2/s and 26.0 W/m K, 9.3 $\times 10^{-6}$ m^2/s, respectively, showing good consistency between the two measurement schemes. It should be mentioned that three parameters in the expanded beam scheme or four parameters in the focused beam scheme are involved in the fitting process. The effective case depth and the effective thermal properties are correlated, as can be seen in Eq. (6). Therefore, it is necessary to know one of the parameters in order the estimate the rest. In our case, once the effective case depth is determined, the fitting of the effective thermophysical properties is unique because different values of the parameters cause different behaviors of the PTR signal, as discussed elsewhere.[18] On the other hand, for a given type of steel, it is possible to reconstruct the case hardened depth directly from the radiometric data in a nondestructive manner based on the fact that the changes in thermophysical properties (thermal conductivity k and thermal diffusivity α)

TABLE I. Fitting results of using different effective case depths.

Coating thickness (μm)	Expanded beam		Focused beam		
	k_c (W/m K)	α_c ($\times 10^{-6}$ m^2/s)	k_c (W/m K)	α_c ($\times 10^{-6}$ m^2/s)	r (mm)
391.5	23.0	6.7	27.0	8.0	0.84
435.1	26.0	9.3	29.4	9.0	0.86
478.5	26.2	9.6	31.5	9.9	0.87

at the surface after hardening with respect to the unhardened bulk are independent of the actual case depth. The effective case depth of such a type of steel can then be determined in a nondestructive way based on a calibration process.[19] Different assumptions regarding the effective thickness of the case depth may affect the fitted thermophysical parameters of the hardened layer. To show the effect of the thickness, we constructed Table I to give the fitted results under the assumption that the effective case depth is in the range between 391.5 and 478.5 μm ($\pm 10\%$ deviation from 436.1 μm). In this thickness range, the best-fitted thermal conductivity and thermal diffusivity of the hardened layer range from 27 to 31.5 W/m K and 8.1×10^{-6} to 9.9×10^{-6} m^2/s for the focused beam, and from 23.0 to 26.2 W/m K and 6.7 to 9.6×10^{-6} m^2/s for the expanded beam, respectively. The range of fitted parameters may represent the approximate change of thermal conductivity and thermal diffusivity of C1018 steel after a standard industrial carbonitride process. It is also seen that the fitted measurement coordinates r remain reasonably consistent, all around $\sim$0.8 mm.

V. CONCLUSIONS

We have investigated the influence of the laser beam size on the measurement sensitivity of thermophysical properties (thermal diffusivity and conductivity) in layered systems consisting of hardened case and substrate steel layers using the PTR technique. The behavior of amplitude and phase under different combinations of thermophysical properties and laser beam sizes was investigated. It was found that these measurements can be used as a quick check of the relative thermophysical properties between the thin-coating layer and the substrate and the theoretical fits to the frequency scan data as benchmarks for the determination of the thermophysical parameters. The beam size effect on PTR measurement sensitivity was also theoretically examined and experimentally demonstrated using a carbonitrided C1018 steel sample. It is concluded both theoretically and experimentally that, for a given sample with a layered structure, an expanded beam usually generates a larger magnitude change in both amplitude and phase channels than a focused beam at low frequencies, which are more reliable in practice than similar features at high frequencies using a focused beam. The latter can be effectively distorted or masked by possible surface roughness, polish, and/or contamination. The goodness of fit to the data demonstrates that continuously varying thermophysical property depth profiles behave like discrete two-layer systems under thermal-wave interrogation and may yield effective thermophysical properties and/or effective case depth in hardened steels.

ACKNOWLEDGMENTS

The authors wish to acknowledge the support of the Ontario Centers of Excellence (OCE) for this project through a Collaborative Contract to A.M. The support of the educational committee of Jiangsu province (Contract No. Q2108608) and an initializing research fund of Suzhou University (Q4108612) are also gratefully acknowledged.

[1] A. Rosencwaig and A. Gersho, J. Appl. Phys. **47**, 64 (1976).
[2] M. Beyfuss, H. Reichl, and J. Baumann, in *Photoacoustic and Photothermal Phenomena III*, Springer Series in Optical Sciences Vol. 69, edited by D. Bicanic (Springer, Heidelberg, 1992), p. 692.
[3] J. Shen and A. Mandelis, Rev. Sci. Instrum. **66**, 4999 (1995).
[4] L. Wei, P. K. Kuo, and R. L. Thomas, *Photoacoustic and Photothermal Phenomena III*, Springer Series in Optical Sciences (in Ref. 2), p. 251.
[5] A. Salazar, A. Sanchez-Lavega, and J. M. Terron, J. Appl. Phys. **84**, 3031 (1998).
[6] T. D. Bennett, and F. Yu, J. Appl. Phys. **97**, 013520 (2005).
[7] P. Z. Li and G. Y. Zhou, Appl. Opt. **31**, 3781 (1992).
[8] J. A. Garcia, A. Mandelis, B. Farahbakhsh, C. Lebowitz, and I. Harris, Int. J. Thermophys. **20**, 1587 (1999).
[9] A. Bendada, M. Lamontagne, and H. Roberge, Int. J. Thermophys. **24**, 207 (2003).
[10] L. Qian and P. Z. Li, Chin. Phys. **11**, 417 (1991).
[11] M. Reichling and H. Gronbeck, J. Appl. Phys. **75**, 1914 (1994).
[12] L. Nicolaides, A. Mandelis, and C. J. Beingessner, J. Appl. Phys. **89**, 7879 (2001).
[13] M. Reichling and H. Grönbeck, J. Appl. Phys. **75**, 1914 (1994).
[14] L. Nicolaides and A. Mandelis, J. Appl. Phys. **90**, 1255 (2001).
[15] A. Salazar, A. Sanchez-Lavega, and J. Fernandez, J. Appl. Phys. **70**, 3031 (1991).
[16] A. Mandelis, *Diffusion-Wave Fields: Mathematical Methods and Green Functions* (Springer, New York, 2001).
[17] *Metals Handbook*, 10th ed. (ASM International, Materials Park, OH, 1990), Vol. 1, p. 196.
[18] C. Wang, A. Mandelis, and Y. Liu, J. Appl. Phys. **97**, 014911 (2005).
[19] C. Wang and A. Mandelis, NDT & E Int. **40**, 158 (2007).